IEEE Photonics Journal
An IEEE Photonics Society Publication

Temperature-Insensitive Magnetic Field Sensor Based on Nanoparticle Magnetic Fluid and Photonic Crystal Fiber

Volume 4, Number 2, April 2012

Peng Zu, Member, IEEE
Chi Chiu Chan, Member, IEEE
Wen Siang Lew
Limin Hu
Yongxing Jin
Hwi Fen Liew
Li Han Chen
Wei Chang Wong
Xinyong Dong, Member, IEEE

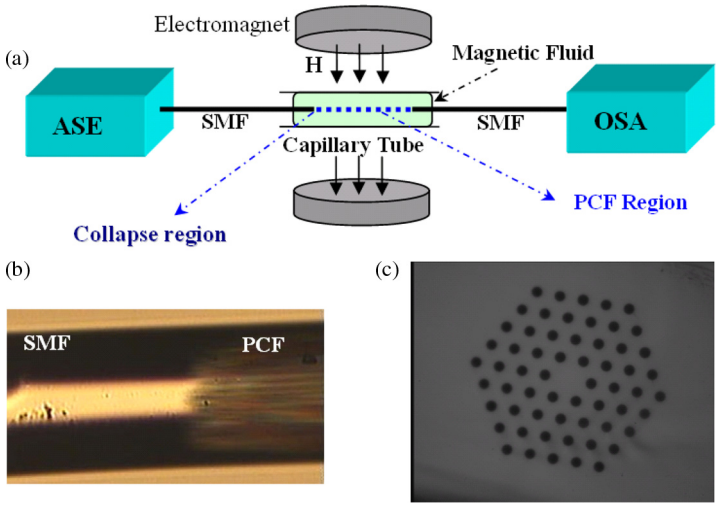

DOI: 10.1109/JPHOT.2012.2192473
1943-0655/$31.00 ©2012 IEEE

Temperature-Insensitive Magnetic Field Sensor Based on Nanoparticle Magnetic Fluid and Photonic Crystal Fiber

Peng Zu,[1] *Member, IEEE*, Chi Chiu Chan,[1] *Member, IEEE*, Wen Siang Lew,[2] Limin Hu,[3] Yongxing Jin,[3] Hwi Fen Liew,[2] Li Han Chen,[1] Wei Chang Wong,[1] and Xinyong Dong,[3] *Member, IEEE*

[1]School of Chemical and Biomedical Engineering, Nanyang Technological University, Singapore 637459
[2]School of Physical and Mathematical Science, Nanyang Technological University, Singapore 637371
[3]Institute of Optoelectronic Technology, China Jiliang University, Hangzhou 310018, China

DOI: 10.1109/JPHOT.2012.2192473

Manuscript received February 21, 2012; revised March 23, 2012; accepted March 23, 2012. Date of current version April 4, 2012. Corresponding author: C. C. Chan (e-mail: eccchan@ntu.edu.sg).

Abstract: A novel magnetic field sensor based on the magnetic fluid and Mach–Zehnder interferometer is proposed. The sensor takes advantage of the tunable refractive index property of the magnetic fluid and the modal interference property of the collapsed photonic crystal fiber. The achieved sensitivity and resolution of the sensor are 2.367 pm/Oe and 4.22 Oe, respectively. The magnetic field sensor is insensitive to the temperature variation with a temperature coefficient of 3.2 pm/°C.

Index Terms: Mach–Zehnder interferometer, magnetic field sensor, magnetic fluid, photonic crystal fiber.

1. Introduction

Magnetooptical sensors are the magnetic field sensors based on the magnetooptical effects of the special magnetic functional materials, which characterized by their capability of working in harsh environment, small size, and so on [1]. In magnetooptical sensors, the magnetooptical materials are the key elements which interact directly or indirectly with the parameters of the light such as light intensity, phase and polarization. Magnetic fluid is such a kind of nanoparticle magnetooptical material which exhibits both the magnetism like solid material and fluidity like liquid material. The magnetic fluid possesses various outstanding magnetooptical effects such as refractive index tunability, linear birefringence, linear dichroism, Faraday effect, magnetochromatic effect, field dependent transmission property, and so on [1]–[5]. Many magnetic fluid-based photonic devices, especially magnetic field fiber sensors, were reported [6]–[9]. For example, Hu demonstrated a magnetic field sensor based on Fabry–Perot interferometer for electric current measurement application [7]. Dai carried out a magnetic field sensor by combining magnetic fluid with the etched fiber Bragg grating (FBG) [6]. In our previous work, magnetooptical sensor and modulator based on Sagnac interferometer were also investigated [9], [10]. Recently, a unique kind of microstructure fiber, photonic crystal fiber (PCF), emerges, which makes the fiber sensors more versatile and designable. The PCFs can be served as a new sensing platform for the magnetic fluid by taking advantage of their air-hole structure. A magnetic filed sensor by inserting the magnetic fluid into the air-holes of the PCF was implemented [8]. Besides, the guiding mode property of PCFs can be modified from single-mode state to multimode state by collapsing the air-holes of PCFs, which was insensitively investigated, too.

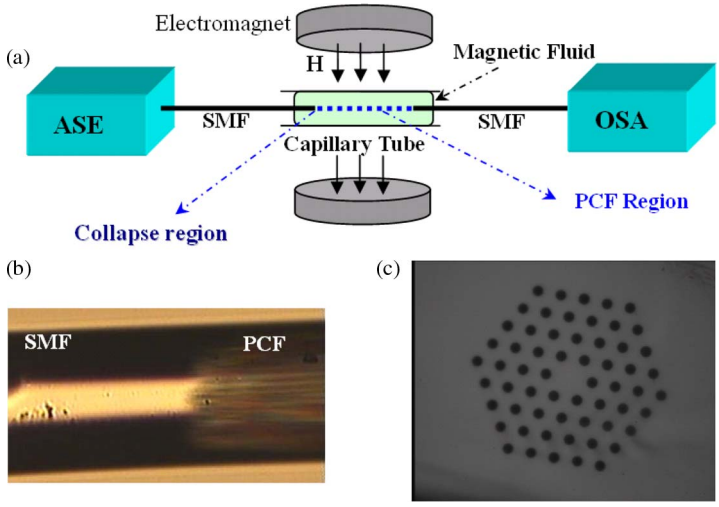

Fig. 1. (a) Diagram of the proposed magnetic field sensor. (b) Splicing point between the photonic crystal fiber and single-mode fiber. The image shows that a collapse region appears at the splicing point. (c) The SEM image of the cross section of the photonic crystal fiber used (LMA-10 Crystal Fiber).

Therefore, modal interference can be generated by collapsing the air-holes of PCF and Mach–Zehnder interferometer based on modal interference of PCF can be formed for various parameter measurements such as strain, microbending, temperature, ambient dielectric environment, and so on [11]–[14].

Hence, in this work, a novel magnetic field sensor that combines the magnetic fluid and Mach–Zehnder interferometer based on the collapsed PCF is proposed.

2. Structure and Fabrication of the Sensor

The configuration of the proposed magnetic field fiber sensor is illustrated in Fig. 1, which is based on a Mach–Zehnder interferometer with the magnetic fluid as its outer cladding layer. The Mach–Zehnder interferometer is a "sandwich" structure which was fabricated simply by splicing a section of 20-mm-length PCF (LMA-10) between two sections of single-mode fibers (SMFs). The PCF was prepared with a mechanical cleaver and spliced with a common commercial available fusion splicer (Fujikura FSM-40S). The default parameters for splicing SMFs were used, but the arc position was slightly moved to the PCF side (about 50 μm) in order to collapse the air-hole cladding of the PCF effectively. Subsequently, the PCF near the splicing point was converted into a solid silica "rod". The overall length of the collapsed region was approximately 300 μm which is shown in Fig. 1(b). The SMF–PCF–SMF sandwich structure, which actually formed an optical Mach–Zehnder interferometer, was inserted into a 30-mm-length glass capillary tube. The glass tube was filled with MF in order to form a magnetic fluid cladding layer outside the sandwich structure and then sealed by UV glue to avoid the magnetic fluid from leaking out. Hence, the size of the sensor head is quite small, and total dimension of the sensor was about Φ2 mm $\times$ 30 mm. It is reported that the length of the sensor can be reduced down to 1.2 mm [14]. Light from a broadband light source (amplified spontaneous emission light source, ASE, 1520–1600 nm) was launched into the sensor from one SMF, and the corresponding transmission spectrum was measured at the other SMF with an optical spectrum analyzer (OSA). The overall configuration was placed amid a uniform magnetic field which was supplied by an electromagnet (EM4-HVA, LakeShore) and measured by a gaussmeter (Model 425, LakeShore). The magnet had two poles of 100 mm diameter, and the air gap between the two poles was fixed at 25 mm in the experiment. The uniform cylindrical volume between the two poles of the magnet was about Φ65 mm $\times$ 25 mm with a uniformity of 0.05%. The fiber sensor was placed in the center of the uniform field zone and the transverse Hall probe of the

gaussmeter was fixed near the sensor head. The external magnetic field was applied perpendicularly to the PCF at the region where the magnetic fluid existed.

The PCF used was a solid core fiber, whose image of scanning electron microscope (SEM) is shown in Fig. 1(c). The PCF has typical hexagonal arrangement of air-holes and four layers of air-holes surrounding the central solid core. The whole fiber was made up of the same material, pure silica. The diameter of the air-hole is 3.04 μm, which is so small that it can quite easily collapse during the fusion process. The sizes of the core, cladding, and mode field are 10 μm, 125 μm, and 7.5 μm, respectively.

A water-based magnetic fluid (EMG605, Ferrotec) with a particle volume concentration of 0.39% was used in the experiment. The nanoparticles in the magnetic fluid are Fe_3O_4, and their nominal sizes are about 10 nm. The magnetic fluid used in the experiment, which was a light-brown translucent solution were prepared by the chemical coprecipitation technique [1]. The magnetic susceptibility and the saturation magnetization strength were 2.96 Gs/Oe and 220 Oe, respectively.

3. Operating Principle of the Sensor

3.1. Refractive Index Tunability of Magnetic Fluid

The magnetic fluid is a special polymer colloidal suspension with high stability. The ultrafine ferromagnetic nanoparticles (i.e., Fe_3O_4) are dispersed uniformly in the liquid carrier with the assistance of the surface surfactants and Brownian motion [15]. The refractive index of the magnetic fluid under zero magnetic field increases on the basis of the intrinsic refractive index of the carrier after dispersing the ferromagnetic nanoparticles into the liquid carrier, which depends on the concentration of the nanoparticles [15]. The magnetic fluid changes from the random homogenous state to the field dependent structural pattern state when an external magnetic field is applied to the magnetic fluid. The nanoparticles in the magnetic fluid agglomerate and further form chains as well as magnetic columns along the direction of magnetic field. During the process of the formation of the magnetic columns, phase separation occurs between the columns and liquid in the magnetic fluid under the external magnetic field, which causes the variation of the effective dielectric constant of the magnetic fluid and, meanwhile, causes the variation of the effective refractive index of the magnetic fluid. The effective dielectric constant of the magnetic fluid is given as [16]

$$\varepsilon_{MF} = \frac{-\varepsilon_c(1-f) - \varepsilon_l(f-1) + \sqrt{[\varepsilon_c(1-f) + \varepsilon_l(f-1)]^2 + 4(1+f)^2\varepsilon_c\varepsilon_l}}{2(1+f)} \tag{1}$$

where ε_c and ε_l are the dielectric constants of the magnetic columns and the liquid phase, respectively. ε_l varies with the external magnetic field strength, but ε_c remains a constant. $f = (A_c/A)/(1 - A_c/A)$, where A_c/A describes the area ratio occupied by the magnetic columns, which is dependent on the external magnetic field strength. Therefore, (1) shows the effective dielectric constant ε_{MF} is a function of magnetic field strength. Considering that $n_{MF} = \sqrt{\varepsilon_{MF}}$, the effective refractive index of the magnetic fluid is a function of the magnetic field strength. In conclusion, the higher the magnetic field strength applied, the greater the phase separation that occurs, and the larger the exhibited effective refractive index of magnetic fluid. Further analysis indicates that the relationship between the n_{MF} and the external magnetic field strength follows Langevin function [2].

3.2. Operating Principle of the Mach–Zehnder Interferometer

The Mach–Zehnder interferometer is actually operated based on modal interference of the collapsed PCF. As shown in Fig. 1, the collapsed region of the PCF due to fusion splicing becomes a short section of "glass rod." Hence, the single-mode condition is no longer satisfied. As light propagates from the SMF to the PCF, the light diffracts and spreads out into the region of "glass rod," and subsequently, some higher order modes are excited which continue propagating into the PCF in the form of cladding modes. Because the effective refractive indices of the cladding modes and core

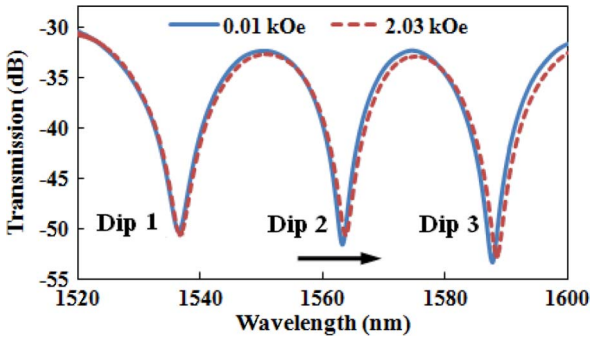

Fig. 2. Transmission spectra of the Mach–Zehnder interferometer under different magnetic field strengths.

mode of the PCF are different, a phase difference is accumulated as the light travels along the length of the PCF. As a result, the core mode and cladding modes recombine and interfere at the second collapsed point, and subsequently, the light after interfering is guided in the following SMF and monitored by the optical spectrum analyzer. The corresponding transmission spectrum is usually analyzed by the two-mode interference model for simplification [14], [17]

$$T(\lambda) = I_{co}(\lambda) + I_{cl}(\lambda) + 2\sqrt{I_{co}(\lambda)I_{cl}(\lambda)}\cos(2\pi\Delta nL/\lambda) \tag{2}$$

where $I_{co}(\lambda)$ and $I_{cl}(\lambda)$ are the intensities of the core mode and first order cladding mode, respectively. Δn is the difference between the effective refractive indices of the core mode and first-order cladding mode. L is the length of PCF, and λ is the operating wavelength. Fig. 2 shows that the transmission spectrum of the Mach–Zehnder interferometer is an approximate sinusoidal function of λ, which indicates that the simplification of two-mode interference model is applicable to this sensor. If the condition $2\pi\Delta nL/\lambda = 2m\pi$ (m is integer) is fulfilled, the transmission spectrum reaches minimum, and a series of transmission dips appear on the transmission spectrum, whose wavelengths are given by

$$\lambda_m = \frac{\Delta nL}{m}. \tag{3}$$

The period of the transmission spectrum S can be given by calculating the space between two adjacent minima

$$S = \frac{\lambda^2}{\Delta nL}. \tag{4}$$

S describes the dynamic measurement range of the sensor. Equation (4) shows S is inversely proportional to the length of PCF. Therefore, larger dynamic measurement range can be achieved by reducing the length of PCF L.

The Mach–Zehnder interferometer is immersed into the magnetic fluid under the external magnetic field to be functionalized as a magnetic field sensor. The cladding modes interact with the magnetic fluid in the form of evanescent field at the outer surface of the PCF, while the core mode is not affected by the dielectric environment of the magnetic fluid. Therefore, as the refractive index of the magnetic fluid is changed with the variation of the magnetic field strength, the effective refractive indices of cladding modes are changed, and in turn, the refractive index difference Δn as well as the phase difference for interference is changed, too. As a result, the transmission spectrum shifts with the change of the external magnetic field strength. Thus, the magnetic field can be measured by monitoring the shift of the spectrum or the wavelengths of the transmission dips. It is worth noticing that the refractive index of magnetic fluid n_{MF} should be smaller than the refractive index of silica ($n_{\text{silica}} = 1.45$) in order to fulfill the condition of total internal reflection. The value of n_{MF} can be controlled by changing the concentration of the magnetic fluid [2], [15].

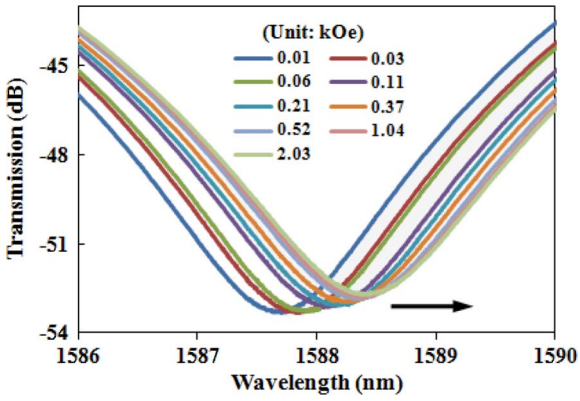

Fig. 3. Dip 3 shifts gradually to the longer wavelength side as the magnetic field strength is increased from 0.01 kOe to 2.03 kOe.

Assuming the refractive index is changed from Δn to $\Delta n'$ due to the variation of the external magnetic field strength, the wavelength shift of the transmission dip $\Delta\lambda_m$, which represents the sensitivity of the sensor, can be given by

$$\Delta\lambda_m = \frac{(\Delta n' - \Delta n)L}{m}. \tag{5}$$

Equation (5) shows that smaller m leads to a larger sensitivity $\Delta\lambda_m$, which is corresponding to the dip at longer wavelength side (i.e., dip 3 shown in Fig. 2). Therefore, we can achieve the highest sensitivity of the sensor by monitoring the dip of the longest wavelength.

4. Experimental results and discussion

The experiment was conducted at the room temperature of 22.7 °C. The transmission spectrum of the sensor under zero magnetic field is shown in Fig. 2, which is indicated by "0.01 kOe." Three transmission dips appeared on the transmission spectrum in the range from 1520 nm to 1600 nm, and the space between the two adjacent dips was about 24.6 nm. The extinction ratio of the transmission spectrum was as high as about 24 dB, which was much better than the results of most sensors based on Mach–Zehnder interferometer of sandwich structure [14], [17]. As the magnetic field strength was increased from 0.01 kOe to 2.03 kOe, the three transmission dips were shifted from 1536.436 nm, 1563.168 nm, and 1587.7 nm to 1536.716 nm, 1563.712 nm, and 1588.436 nm, respectively; the corresponding total wavelength shift were 0.280 nm, 0.544 nm, and 0.736 nm, respectively. The extinction ratio remained almost unchanged. It can be seen that the highest sensitivity is obtained from the dip 3. Thus, the dip 3 was chosen as an example to show the transmission dip shifts gradually to the longer wavelength side with the variation of the external magnetic field strength in details in Fig. 3. After the external magnetic field strength was removed, the transmission spectrum shifted back to the original position. It shows that the magnetic fluid is superparamagnetic and exhibits no hysteresis effect [10], which means the sensor has a good repeatability.

In order to investigate the sensitivity of the sensor, the relationships between the wavelength shifts of all the three dips and variation of the magnetic field strength are shown in Fig. 4. It indicates that the variation trends for the three transmission dips are similar as the magnetic field strength increases, which are all can be fit by modified Langevin function with high R^2 values, but the wavelength shift ranges are different, and the dip 3 has the largest wavelength shift range. For each of these three dips, the wavelength shift continues increasing as the magnetic field strength increases; when the magnetic field strength is smaller than a certain value (saying, $H < 0.3$ kOe), the wavelength shift increases linearly and quickly as the increase of the magnetic field strength; when the magnetic field strength is increased larger than a certain value (saying, $H > 0.5$ kOe), the

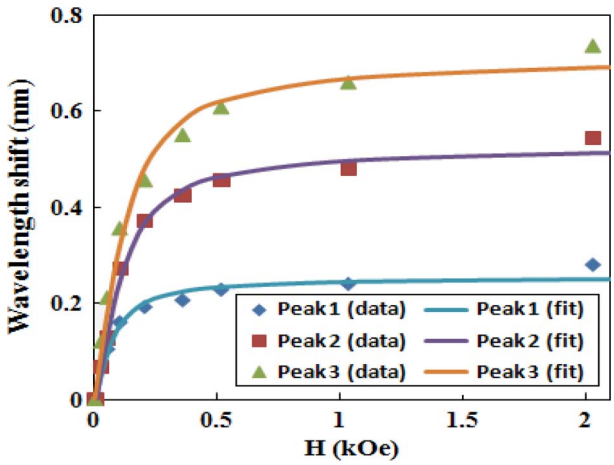

Fig. 4. Relationships between the dip wavelength shifts of all the three transmission dips and the variation of the magnetic field strength.

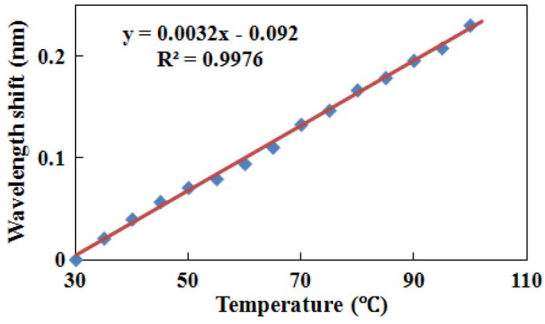

Fig. 5. Relationship between wavelength shift of dip 3 and variation of magnetic field strength in the temperature range from 30 °C to 100 °C.

wavelength shift tends to get saturated gradually; when the magnetic field strength is between the two certain values (saying, 0.3 kOe < H < 0.5 kOe), the wavelength shift is in a period of transition from linear region to saturated region. The linear fit method is applied to the linear variation section of all the three curves. The achieved corresponding sensitivities for the dip 1, dip 2, and dip 3 are 1.012 pm/Oe, 1.927 pm/Oe, and 2.367 pm/Oe, respectively. The dip 3, at the longest wavelength, has the best sensitivity, which is coincident as the theory predicts. For the dip 3, the sensitivity is twice as good as the result of sensor based on Fabry–Perot interferometer, which was about 1.25 pm/Oe [7] and one order of magnitude better than the result of the magnetic field sensor based on etched FBG, which was about 0.344 pm/Oe [6]. If the resolution limit of the optical spectrum analyzer (10 pm) is considered, the corresponding resolutions for the dip 1, dip 2, and dip 3 are 9.88 Oe, 5.19 Oe, and 4.22 Oe, respectively.

Another distinguished advantage of PCF over conventional fiber is the ultralow temperature coefficient because it is made up of identity material, i.e., fused silica; thus, the PCF can avoid the problems caused by the different thermal expansion coefficients existing in the core and cladding area of the conventional fiber. The temperature stability of the sensor was tested in the experiment, too. The overall sensor was placed into a temperature-controlled oven. The temperature was measured by a digital thermometer with an accuracy of ±0.5%. The sensor was heated in the oven, and then, the corresponding transmission spectrum was measured after the temperature was stable. The wavelength shift was recorded as the temperature increased from 30 °C to 100 °C with an interval of 5 °C and the result is shown in Fig. 5. During the process of the increase in

temperature, the wavelength shift increases linearly from 1587.702 nm to 1587.933 nm, which is totally about 0.231 nm to the longer wavelength side. A linear fit is applied to the data with a high R^2 value of 0.9976, which means the temperature dependence of the sensor has a highly linear relationship. The linear fit function of the data can be used to compensate wavelength shift deviation caused by the environmental temperature. The temperature-dependent coefficient of the sensor is calculated to be 3.2 pm/°C, which is about 3 orders of magnitude better than the result of conventional fiber, which is about 1 nm/°C [18]. However, the temperature coefficient is comparable to the sensitivity of the magnetic field sensor, and if the environmental temperature variation range is larger than 1 °C, it is better that the temperature compensation is applied for the sensing measurement.

5. Conclusion

In conclusion, a magnetic field fiber sensor based on the Mach–Zehnder interferometer and the magnetic fluid is proposed and demonstrated. The modal interference phenomenon is achieved by using the two collapse points of air-hole cladding on the length of the PCF to form the Mach–Zehnder interferometer, whose evanescent field is sensitive to the ambient dielectric constant and refractive index in the environment. Moreover, the magnetic fluid is such a nanostructure function material that its dielectric constant and refractive index is tunable under external magnetic field. Hence, the proposed magnetic field fiber sensor is configured by combining Mach–Zehnder interferometer and tunable refractive index property of magnetic fluid. Theoretical analysis of the operating principle indicates that higher sensitivity can be achieved by using lower order interference fringe of the spectrum and the experimental results support this conclusion. The achieved sensitivity and resolution are 2.367 pm/Oe and 4.22 Oe, respectively. The ultralow temperature-dependence coefficient of the sensor is 3.2 pm/°C. The sensor structure is simple, robust, and easy to manufacture. Although the splicing points of PCF may slightly differ from time to time, the modal interference phenomenon is repeatable; hence, the sensing performance is not affected. The sensor can also find some potential applications such as magnetooptical modulation, magnetooptical filters, and so on.

References

[1] L. Martinez, F. Cecelja, and R. Rakowski, "A novel magneto-optic ferrofluid material for sensor applications," *Sens. Actuators A, Phys.*, vol. 123/124, pp. 438–443, Sep. 2005.

[2] C. Y. Hong, H. E. Horng, and S. Y. Yang, "Tunable refractive index of magnetic fluids and its applications," in *Proc. Physica Status Solidi C: Magnetic and Superconducting Materials*, M. Stutzmann, Ed. Weinheim, Germany: Wiley-VCH Verlag Gmbh, 2004, pp. 1604–1609.

[3] H. E. Horng, S. Y. Yang, S. L. Lee, C. Y. Hong, and H. C. Yang, "Magnetochromatics of the magnetic fluid film under a dynamic magnetic field," *Appl. Phys. Lett.*, vol. 79, no. 3, pp. 350–352, Jul. 2001.

[4] H. E. Horng, C. S. Chen, K. L. Fang, S. Y. Yang, J. J. Chieh, C. Y. Hong, and H. C. Yang, "Tunable optical switch using magnetic fluids," *Appl. Phys. Lett.*, vol. 85, no. 23, pp. 5592–5594, Dec. 2004.

[5] M. Xu and P. J. Ridler, "Linear dichroism and birefringence effects in magnetic fluids," *J. Appl. Phys.*, vol. 82, no. 1, pp. 326–332, Jul. 1997.

[6] J. X. Dai, M. H. Yang, X. B. Li, H. L. Liu, and X. L. Tong, "Magnetic field sensor based on magnetic fluid clad etched fiber Bragg grating," *Opt. Fiber Technol.*, vol. 17, no. 3, pp. 210–213, May 2011.

[7] T. Hu, Y. Zhao, X. Li, J. Chen, and Z. Lv, "Novel optical fiber current sensor based on magnetic fluid," *Chin. Opt. Lett.*, vol. 8, no. 4, pp. 392–394, Apr. 2010.

[8] H. V. Thakur, S. M. Nalawade, S. Gupta, R. Kitture, and S. N. Kale, "Photonic crystal fiber injected with Fe_3O_4 nanofluid for magnetic field detection," *Appl. Phys. Lett.*, vol. 99, no. 16, p. 161 101, Oct. 2011.

[9] P. Zu, C. C. Chan, L. W. Siang, Y. X. Jin, Y. F. Zhang, L. H. Fen, L. H. Chen, and X. Y. Dong, "Magneto-optic fiber Sagnac modulator based on magnetic fluids," *Opt. Lett.*, vol. 36, no. 8, pp. 1425–1427, Apr 2011.

[10] P. Zu, C. C. Chan, W. S. Lew, Y. Jin, Y. Zhang, H. F. Liew, L. H. Chen, W. C. Wong, and X. Dong, "Magneto-optical fiber sensor based on magnetic fluid," *Opt. Lett.*, vol. 37, no. 3, pp. 398–400, Jan. 2012.

[11] H. Y. Choi, M. J. Kim, and B. H. Lee, "All-fiber Mach–Zehnder type interferometers formed in photonic crystal fiber," *Opt. Exp.*, vol. 15, no. 9, pp. 5711–5720, Apr. 2007.

[12] G. A. Cardenas-Sevilla, V. Finazzi, J. Villatoro, and V. Pruneri, "Photonic crystal fiber sensor array based on modes overlapping," *Opt. Exp.*, vol. 19, no. 8, pp. 7596–7602, Apr. 2011.

[13] K. S. Park, H. Y. Choi, S. J. Park, U. C. Paek, and B. H. Lee, "Temperature robust refractive index sensor based on a photonic crystal fiber interferometer," *IEEE Sens. J.*, vol. 10, no. 6, pp. 1147–1148, Jun. 2010.

[14] H. P. Gong, C. C. Chan, Y. F. Zhang, W. C. Wong, and X. Y. Dong, "Miniature refractometer based on modal interference in a hollow-core photonic crystal fiber with collapsed splicing," *J. Biomed. Opt.*, vol. 16, no. 1, p. 017 004, Jan. 2011.
[15] H. E. Horng, C. Y. Hong, S. Y. Yang, and H. C. Yang, "Designing the refractive indices by using magnetic fluids," *Appl. Phys. Lett.*, vol. 82, no. 15, pp. 2434–2436, Apr. 2003.
[16] S. Y. Yang, J. J. Chieh, H. E. Horng, C. Y. Hong, and H. C. Yang, "Origin and applications of magnetically tunable refractive index of magnetic fluid films," *Appl. Phys. Lett.*, vol. 84, no. 25, pp. 5204–5206, Jun. 2004.
[17] R. Jha, J. Villatoro, G. Badenes, and V. Pruneri, "Refractometry based on a photonic crystal fiber interferometer," *Opt. Lett.*, vol. 34, no. 5, pp. 617–619, Mar. 2009.
[18] O. Frazão, J. Baptista, and J. Santos, "Recent advances in high-birefringence fiber loop mirror sensors," *Sensors*, vol. 7, no. 11, pp. 2970–2983, Nov. 2007.